Catalysis Today 171 (2011) 24–35

Contents lists available at ScienceDirect

Catalysis Today

journal homepage: www.elsevier.com/locate/cattod

$LaNiO_3$ perovskite catalyst precursor for rapid decomposition of methane: Influence of temperature and presence of H_2 in feed stream

T. Maneerung, K. Hidajat, S. Kawi*

Department of Chemical & Biomolecular Engineering, National University of Singapore, 4 Engineering Drive 4, Blk E5 #02-09, Singapore 117576, Singapore

ARTICLE INFO

Article history:
Received 28 October 2010
Received in revised form 23 March 2011
Accepted 29 March 2011
Available online 31 May 2011

Keywords:
Rapid decomposition of methane
$LaNiO_3$ perovskite
Hydrogen production
Carbon nanotube
Encapsulating carbon
Rapid deactivation

ABSTRACT

$LaNiO_3$ perovskite has been successfully used as a crystalline catalyst precursor for the rapid decomposition of methane into carbon nanotubes (CNTs) and CO_x-free H_2. The advantages of $LaNiO_3$ perovskite, when compared with Ni-supported La_2O_3 catalyst, are as follows: (1) its ability to perform at higher reaction temperature to achieve higher CH_4 conversion, ~90% CH_4 conversion at 800 °C vs. only 55% at 650 °C for NiO/La_2O_3 catalyst; (2) no significant deactivation of $LaNiO_3$ catalyst; and (3) its ability to maintain catalytic activity for a long reaction time due to its ability to form CNTs even at high reaction temperature, while Ni-supported La_2O_3 catalyst mostly started forming encapsulating carbon species at 650 °C which caused rapid deactivation of catalyst. CNTs obtained from $LaNiO_3$ perovskite have highly uniform diameter of 24 nm, which is the same size as Ni^0 particles after the reduction of $LaNiO_3$ perovskite catalyst. Moreover, the presence of H_2 (10 vol%) in the feed stream not only reduces the deactivation rate of $LaNiO_3$ perovskite catalyst at high reaction temperature, but also eliminates amorphous carbon on the surface of CNTs and improves the ordered graphitic structure of CNTs.

1. Introduction

Hydrogen (H_2) is an attractive alternative fuel source since it is an ultra-clean energy and water is the only emission product from its combustion. Currently, there are several catalytic processes for the production of H_2 from methane:

- Steam reforming [1]: $CH_4 + H_2O \leftrightarrow 3H_2 + CO$ (ΔH_{298} = +206 kJ mol^{-1})
- Dry reforming [2]: $CH_4 + CO_2 \leftrightarrow 2H_2 + 2CO$ (ΔH_{298} = +247 kJ mol^{-1})
- Partial oxidation of methane [3]: $CH_4 + (1/2)O_2 \leftrightarrow 2H_2 + CO$ (ΔH_{298} = −8.5 kJ mol^{-1})

However, these processes produce H_2 in the form of synthesis gas (mixture of H_2 and CO) with small amount of CO_2. Therefore, the additional downstream processes such as water-gas shift reaction ($CO + H_2O \leftrightarrow H_2 + CO_2$), CO_2 removal as well as separation process are thus required to minimize the amount of CO_x-species in the purified H_2, due to the greenhouse effect of CO_2 and CO poisoning of Pt-catalyst in the fuel cell application.

From these facts, catalytic decomposition of methane (CDM, $CH_4 \rightarrow 2H_2 + C$) can be considered as the alternative route of CO_x-free H_2 production. In this CDM reaction, methane is decomposed only to H_2 and solid carbon, thereby eliminating the requirement of the additional downstream processes. This solid carbon can also be produced in a highly valuable form of carbon nanotubes (CNTs) which have been studied for many applications ever since it has been found by Iijima [4], such as hydrogen storage, electronic components, polymer additives, catalyst support or direct catalyst [5–8]. The mechanism of the formation of CNTs during CDM reaction, which has been intensively studied in the past [9,10], has been proposed as follows: (1) methane is decomposed on the front surface of metal particle followed by the dissolution of carbon atoms; (2) dissolved carbon atoms diffuse through metal particle; and (3) finally, the dissolved carbon atoms precipitate in the form of graphite at the rear of metal particle, consequently detaching the metal particle from the support and forming CNT with the exposed metal particle at its tip. According to this mechanism known as tip-growth mechanism, metal particle at the tip is always clean enough to react with methane, thus allowing catalysts to maintain their activities in spite of increasing concentration of carbon deposited on the catalysts.

Catalysts being studied in this process mainly consist of transition metals such as Ni, Co, and Fe [11–13]. Ni-based catalysts are known to be the most effective due to its high activity for reforming methane and its ability to form CNTs at moderate temperature [14]. The reported operating temperatures for Ni-supported catalysts ranged from 500 to 900 °C with the maximum methane conversion of 67% at 700 °C [15,16]. Although the Ni-supported

* Corresponding author. Tel.: +65 6516 6312; fax: +65 6779 1936.
E-mail address: chekawis@nus.edu.sg (S. Kawi).

0920-5861/$ – see front matter © 2011 Elsevier B.V. All rights reserved.
doi:10.1016/j.cattod.2011.03.080

catalysts exhibited high activities at moderate reaction temperature (500–700 °C), but their activities at higher reaction temperatures rapidly decreased. This is mainly due to the formation of large agglomerated Ni^0 particles on supports at such high temperatures, which would prefer to form encapsulating carbon instead of CNTs on the catalyst surface. It is thus desirable to develop catalysts with appropriate and uniformed particle size which can be performed at high reaction temperatures to achieve high methane conversion (or high H_2 purity), and at the same time to be able to form CNTs during reaction in order to maintain the catalytic activity for a long period of reaction time.

Perovskite and perovskite-like oxides have been extensively developed as catalyst precursors for many reactions, such as NH_3 oxidation, reforming of methane, and production of CNTs from CVD reaction [17–20]. The main advantage of using either perovskite or perovskite-like oxide as catalyst precursor is the formation of very small and uniformed particle size catalyst which can provide an excellent catalytic performance. In the case of $LaNiO_3$ perovskite, the reducible element (Ni^{3+}) in the perovskite structure can easily be reduced to metallic Ni^0 dispersed on La_2O_3 under appropriate H_2 reduction condition.

In this work, $LaNiO_3$ perovskite was used as a catalyst precursor for co-production of CNTs and CO_x-free H_2 from the rapid decomposition of methane. The ability of $LaNiO_3$ perovskite was investigated to perform at high reaction temperature (up to 800 °C) in order to achieve the higher CH_4 conversion with a much longer period of catalytic life, as well as its ability to form CNTs during the reaction at such high reaction temperatures. Moreover, the effect of H_2 presence in the feed stream on the catalytic performance of $LaNiO_3$ perovskite as well as the ordered structure of obtained CNTs was also investigated.

2. Experimental

2.1. Catalyst preparation

$LaNiO_3$ perovskite catalysts were prepared from the citrate sol–gel method. $La(NO_3)_3{\cdot}6H_2O$ (Sigma–Aldrich) and $Ni(NO_3)_3{\cdot}6H_2O$ (Stem Chemicals) as the metal precursors were weighted in the appropriated amount and dissolved in the distilled water. Citric acid (Sigma–Aldrich) as a chelating agent was then added to the aqueous solution of metal nitrates at 1:1 molar ratio of total cations (La^{3+} and Ni^{3+}) to citric acid. The resulting solution was continually stirred at 55 °C for 6 h until the greenish gel was obtained. This gel was then dried at 100 °C for 24 h. The obtained solid precursor was milled and finally decomposed in air at 400 °C for 1 h using a heating rate of 2 °C/min and subsequently calcined in air at 850 °C for 6 h using a heating rate of 2 °C/min.

NiO/La_2O_3 as a reference supported catalysts, containing the same Ni amount as $LaNiO_3$ perovskite catalysts (i.e. 24 wt%), were prepared by the wet impregnation method. $Ni(NO_3)_3{\cdot}6H_2O$ was weighted and dissolved in the distilled water. After the complete dissolution, the appropriate amount of La_2O_3 (Sigma–Aldrich) was added under continuous stirring. The resulting solution was then heated up to 70 °C to evaporate water. The residue was dried at 100 °C for 24 h and subsequently, calcined in air at 850 °C for 6 h by heating rate of 2 °C/min.

2.2. Catalytic activity testing

The catalytic decomposition of methane (CDM) was performed in a fixed-bed plug flow reactor. All catalysts were placed in the constant temperature zone of a horizontal quartz tube reactor (inner diameter of 4 mm, outer diameter of 6 mm, and length 60 cm). Before the reaction was performed, the catalyst precursor was reduced under a hydrogen atmosphere (flow rate of 20 ml/min) at 600 °C for 1 h. After the reduction, the catalytic decomposition of methane was conducted at three different reaction temperatures, i.e., 600 °C, 700 °C, and 800 °C, in the undiluted methane (99.5% purity) at a flow rate of 20 ml/min. The composition of the gaseous product from the reactor was continually analyzed by the online gas chromatography (GC, HP6890) using a packed column (Carboxen™ 1000, 60/80 mesh sizes and 0.5 g/ft packing density) and a thermal conductivity detector (TCD). The carbon solid was also collected and characterized after the reaction.

2.3. Characterizations

Structure of catalysts was characterized by powder X-ray diffraction using SHIMADZU XRD-600 diffractometer with Cu K_α radiation (λ = 0.154 nm), operated at 40 kV and 30 mA. The data was collected at 0.02° with a counting time of 5 s per step, in the 2θ range of 20–80°.

Reduction behavior of the fresh catalysts was studied by H_2-Temperature Programmed Reduction (H_2-TPR) using a ChemBET™3000. A 50 mg of catalyst was placed in the U-shaped quartz tube. The sample was first degassed at 150 °C for 3 h with the helium flow rate of 50 ml/min and then cooled down to room temperature under the flow of helium. Reduction profiles were recorded using 5 vol% hydrogen in nitrogen, with heating rate of 10 °C/min, from room temperature to 800 °C. Hydrogen consumption was obtained from the integrated peak area of the reduction profiles relative to the calibration curve.

The presence of lattice oxygen in the reduced catalyst precursors was studied by O_2-Temperature Programmed Desorption (O_2-TPD) using a ChemBET™3000. A 100 mg of catalyst was placed in the U-shaped quartz tube. The sample was first reduced under a hydrogen atmosphere (flow rate of 20 ml/min) at 600 °C for 1 h and then cooled down to room temperature under the flow of helium. The O_2-TPD profiles were recorded under the flow of helium (20 ml/min), with heating rate of 10 °C/min, from room temperature to 950 °C.

Morphology of the fresh and the spent catalyst precursors were investigated by Scanning Electron Microscopy (SEM, JEOL 2872), carried out using an electron beam of 15 kV with magnifications in the range of 2000–5000×. The structural properties of the obtained CNTs were further investigated by Transmission Electron Microscopy (TEM, JEOL JEM-2010). The specimens for TEM were prepared by dispersing the samples in ethanol. The resulting mixture was ultrasonicated for 30 s to obtain a homogeneous dispersion after which a droplet of this dispersion was applied on a carbon coated copper grid, followed by drying at 60 °C for 15 min. The microscope was then operated at an acceleration voltage of 100–150 kV, with magnifications in the range of 10,000–100,000×.

3. Results and discussion

3.1. Catalyst characterizations

3.1.1. X-ray diffraction analysis

Fig. 1 shows the XRD patterns of fresh, reduced, and used $LaNiO_3$ perovskite catalyst precursors. Only the characteristic diffraction peaks of perovskite-type structure with a rhombohedral symmetry are observed in the fresh $LaNiO_3$ perovskite catalyst calcined under air at 800 °C for 7 h. However, the NiO phase as the impurity phase can also be detected when the precursor of $LaNiO_3$ perovskite was calcined at the lower temperatures (600 and 700 °C). This result indicates that the highly crystalline and well-defined $LaNiO_3$ perovskite precursor without the impurity phase of NiO can be obtained after the calcination under air at 800 °C for 7 h.

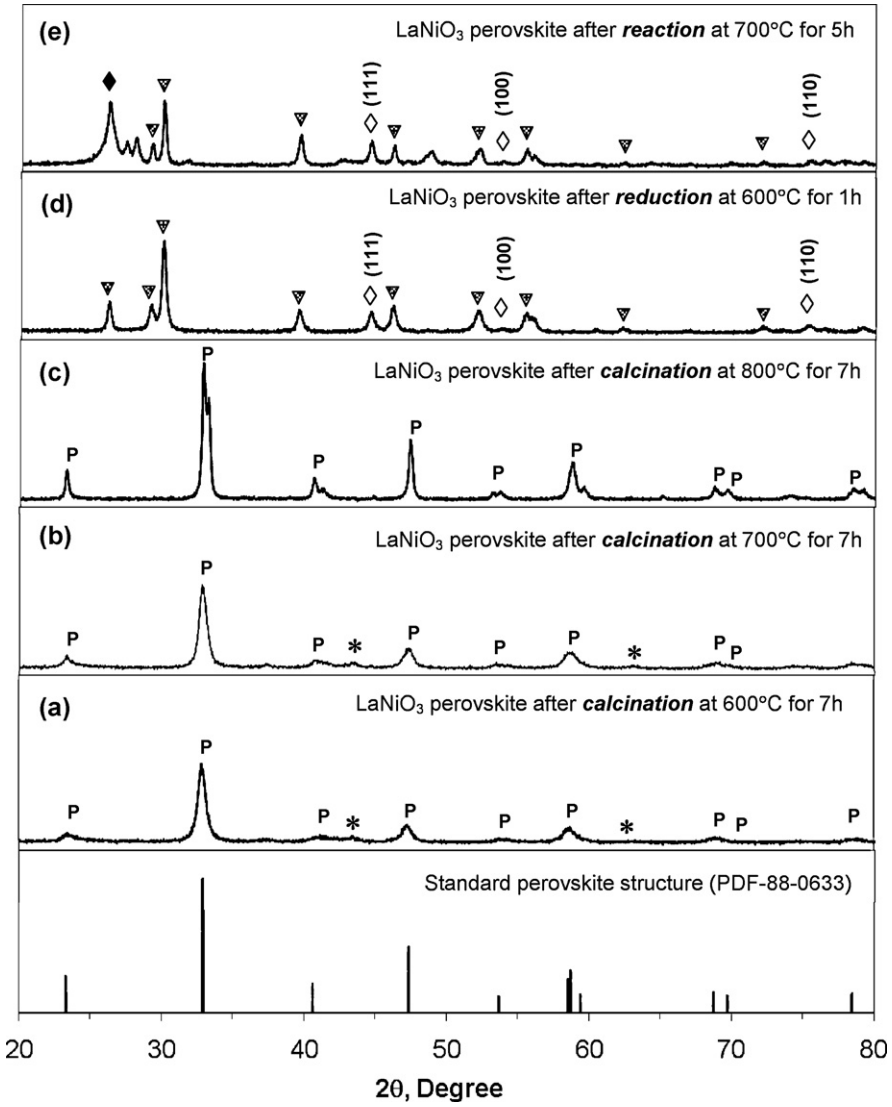

Fig. 1. XRD patterns of the fresh, reduced, and used $LaNiO_3$ perovskite catalyst. ((P) $LaNiO_3$ perovskite, (*) NiO, (◊) metallic Ni^0, (▽) La_2O_3, (♦) Graphite).

Fig. 2 shows the XRD patterns of fresh, reduced, and used NiO/La_2O_3 catalysts. The main characteristic diffraction peaks of the NiO and La_2O_3 phases are observed in the fresh NiO/La_2O_3 catalyst calcined under air at 600 °C for 7 h. In addition to the dominant NiO and La_2O_3 phases, the $LaNiO_3$ perovskite phase can also be detected when the precursor of NiO/La_2O_3 catalyst was calcined at higher temperatures (700 and 800 °C). These results indicate that the solid-state reaction between NiO and surface layer of La_2O_3 occurs during the calcination under air at high temperature, yielding $LaNiO_3$ perovskite as the minor impurity phase.

After the reduction in the H_2 atmosphere at 600 °C for 1 h, the characteristic diffraction peaks attributed to the rhombohedral structure of $LaNiO_3$ perovskite disappear. On the other hand, the characteristic diffraction peaks of La_2O_3 and metallic Ni^0 ($2\theta = 45°$, 52°, and 76.5°) appear (Fig. 1(d)). The formation of metallic Ni^0 is also observed in the NiO/La_2O_3 catalyst after the reduction in the same condition (Fig. 2(d)). Therefore, it can be concluded that whatever the starting catalysts, their starting structures completely collapse and, consequently form the metallic Ni^0 particles dispersed on La_2O_3 under the reduction in the H_2 atmosphere.

3.1.2. The reduction behaviors of catalysts

Fig. 3 shows the reduction behaviors of $LaNiO_3$ perovskite and NiO/La_2O_3 catalyst precursors as observed during H_2-TPR analysis. The H_2-TPR profile of NiO/La_2O_3 (Fig. 3(a)) shows one main transition peak at a temperature range between 300 and 500 °C. This peak is attributed to the reduction of the amorphous NiO phase to the metallic Ni^0 particle [21]:

$$NiO/La_2O_3 + H_2 \rightarrow Ni^0 + La_2O_3 + H_2O$$

Besides the main peak, a very weak and broad shoulder peak is also observed at the higher temperature (around 600 °C). This peak can be assigned to the reduction of $LaNiO_3$ perovskite, confirming the formation of trace amount of perovskite phase at high calcination temperature as similarly observed by XRD.

As for the $LaNiO_3$ perovskite, Fig. 3(b) shows two main peaks at temperature ranges of 300–450 °C and 500–600 °C, respectively. The presence of these two phase transition peaks of $LaNiO_3$ perovskite during the reduction is consistent with the literature result [22], and has been proposed to proceed by the following two phase transition schemes:

$$2LaNiO_3 + H_2 \rightarrow La_2Ni_2O_5 + H_2O$$

$$La_2Ni_2O_5 + 2H_2 \rightarrow 2Ni^0 + La_2O_3\,2H_2O$$

The first transition peak can be assigned to the reduction of Ni^{3+} in the $LaNiO_3$ phase to Ni^{2+} in the $La_2Ni_2O_5$ intermediate phase.

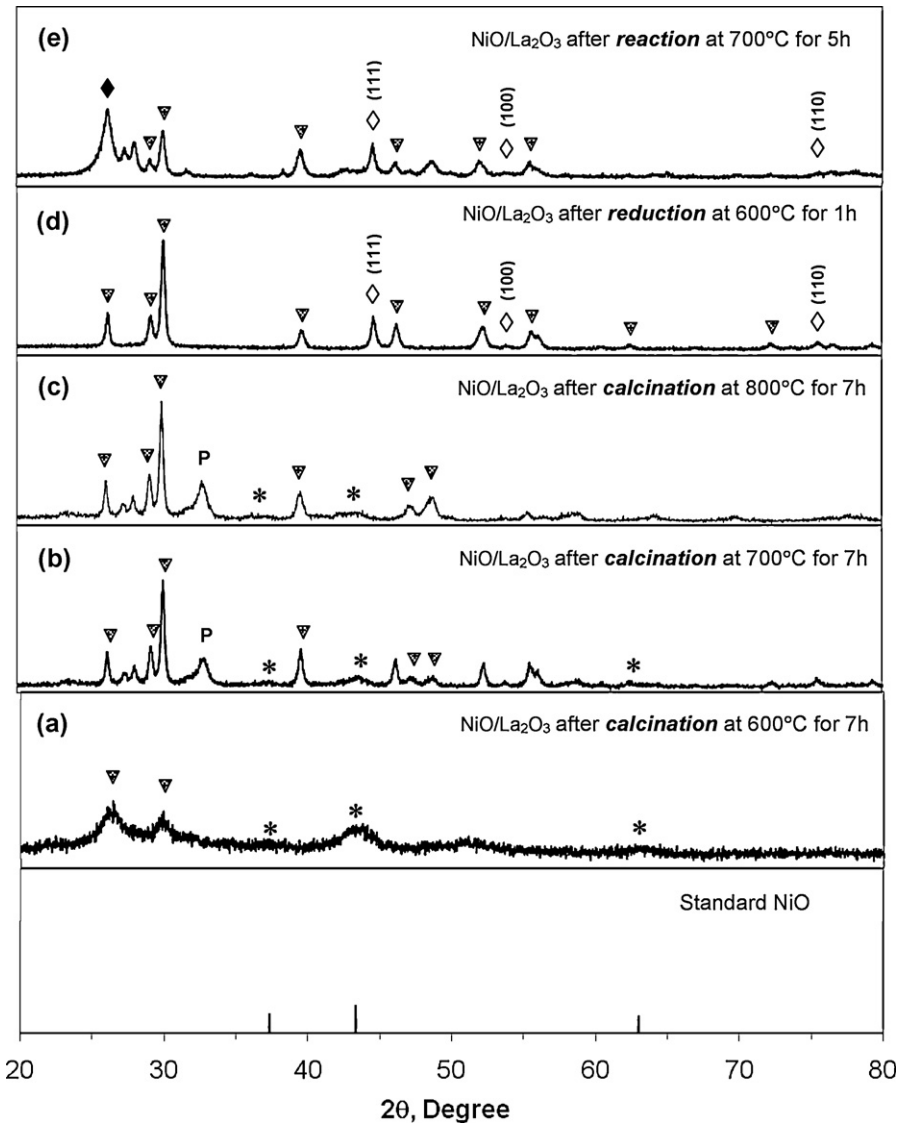

Fig. 2. XRD patterns of the fresh, reduced, and used NiO/La_2O_3 catalyst. ((P) $LaNiO_3$ perovskite, (*) NiO, (◊) metallic Ni^0, (▼) La_2O_3, (♦) Graphite).

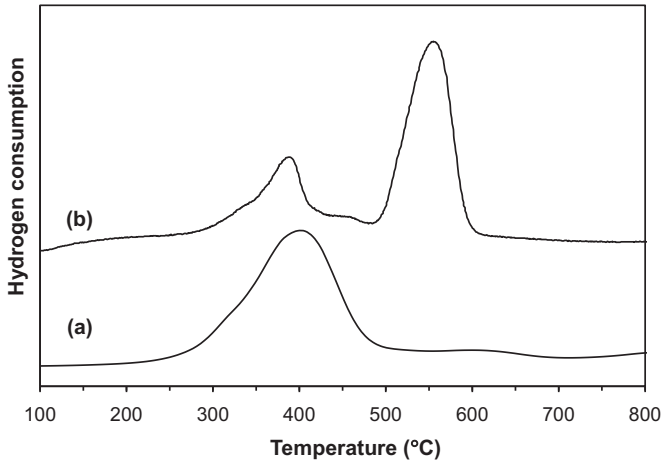

Fig. 3. H_2-TPR profiles of (a) NiO/La_2O_3 and (b) $LaNiO_3$ perovskite.

The second transition peak at higher temperature can be assigned to the reduction of Ni^{2+} to the metallic Ni^0 particles dispersed on La_2O_3. Moreover, the ratio of the area representing H_2 consumption under these two transition peaks is estimated to be 1:2, which corresponds well to the above phase transition schemes. From this H_2-TPR result, it can be concluded that $LaNiO_3$ perovskite has lower reducibility when compared to NiO/La_2O_3, revealing the stronger interaction between nickel atom and lanthanum oxide in the framework of perovskite structure. This stronger interaction between nickel atom and lanthanum oxide hinders the thermal agglomeration of the metallic Ni^0 particles. Therefore, during the reduction in the H_2 atmosphere, nickel atoms emerge from the framework of perovskite and consequently form highly dispersed metallic Ni^0 particles on La_2O_3. On the contrary, NiO weakly interact with La_2O_3 in the NiO/La_2O_3, causing the metallic Ni^0 particles easily susceptible to the thermal agglomeration at high temperatures.

Fig. 4 shows the TEM images characterizing the metallic Ni^0 particles formed on these two catalyst precursors. The Ni^0 particles obtained from the reduction of NiO/La_2O_3 have less uniform and larger particle size (40.78 ± 12.53 nm) than the Ni^0 particles obtained from the reduction of $LaNiO_3$ perovskite

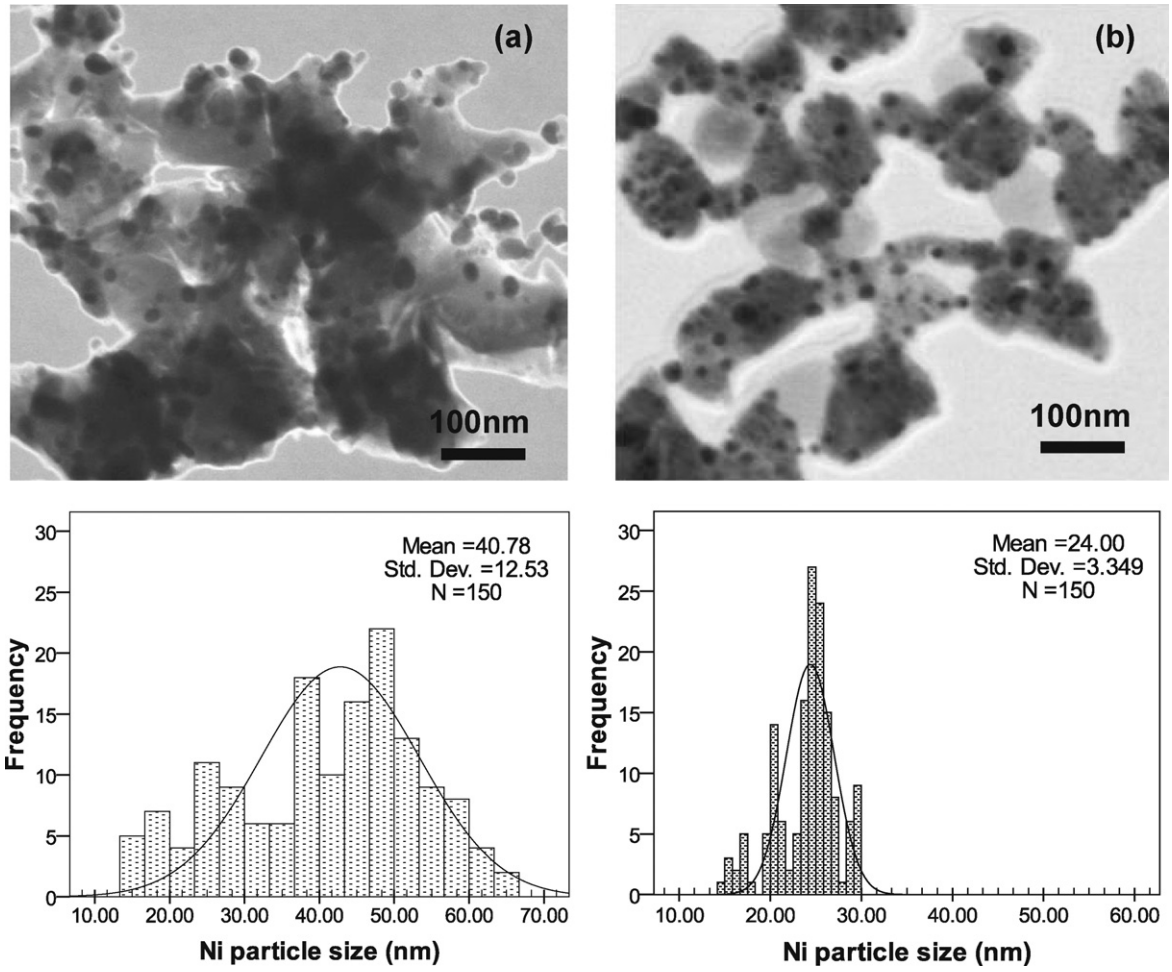

Fig. 4. TEM images and Ni^0 particle size distribution of (a) NiO/La_2O_3 and (b) $LaNiO_3$ perovskite after reduction at 600 °C for 1 h (dark spot represents Ni^0 particles).

(24.00 ± 3.35 nm). These results suggest that the strong interaction between nickel atom and lanthanum oxide in the framework of perovskite can prevent the thermal agglomeration of Ni particles and promote the well dispersion of Ni particles on La_2O_3 after the reduction; this observation is in good agreement with the literature result which reports the advantages of using highly dispersed Ni^0 particles prepared from $LaNiO_3$ perovskite as a catalyst precursor for production of uniformed CNTs [11].

3.2. Catalytic activity for catalytic decomposition of methane

Catalytic decomposition of methane (CDM), which is a mildly endothermic reaction [23], was performed over $LaNiO_3$ perovskite and NiO/La_2O_3 as a reference catalyst in a fixed-bed plug flow reactor at different temperatures. Theoretically, the deposited carbon (C) and hydrogen (H_2) should be the only two products from this CDM reaction:

$$CH_4 \rightarrow C + 2H_2 \quad \Delta H = +74.5\,kJ\,mol^{-1}$$

However, less than 0.2 vol% of carbon monoxide (CO) in the gaseous effluent was also observed only at the beginning of the reaction. The formation of this traceable amount of CO during the CDM reaction with no oxygen in the feed stream is due to the reaction between carbon atoms and lattice oxygen of La_2O_3 support [24,25] as shown in Fig. 8(C). The presence of lattice oxygen (O^{2-}) can be observed at 650 °C from the O_2-TPD profiles of the reduced $LaNiO_3$ perovskite and NiO/La_2O_3 catalyst precursors as shown in Fig. 5.

Fig. 6 shows the catalytic performances of $LaNiO_3$ perovskite and NiO/La_2O_3 catalyst precursors at different reaction temperatures. The catalytic behaviors of $LaNiO_3$ perovskite in the CDM reaction (Fig. 6(a)) are slightly different from those of NiO/La_2O_3 at the beginning of reaction. This is probably due to the $LaNiO_3$ perovskite phase which was incompletely reduced prior to the reaction. The remaining $LaNiO_3$ perovskite phase could be further reduced by

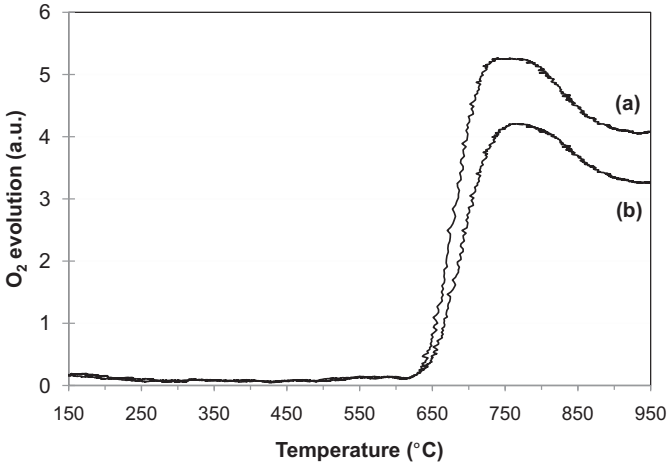

Fig. 5. O2-TPD profiles of (a) NiO/La_2O_3 and (b) $LaNiO_3$ perovskite after reduction under H_2 at 600 °C for 1 h.

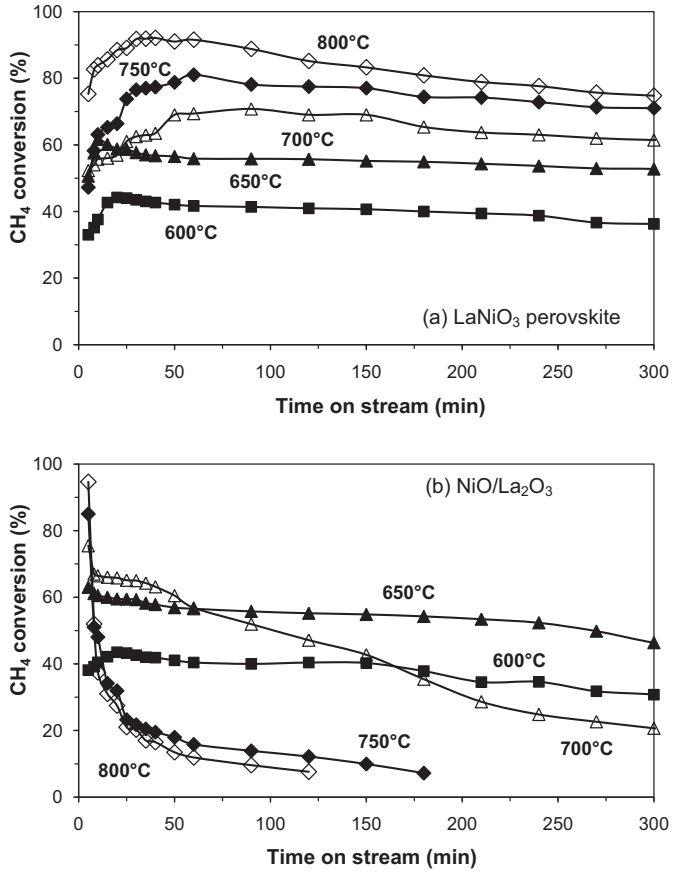

Fig. 6. Time on stream (TOS) vs. % CH_4 conversion over (a) $LaNiO_3$ perovskite and (b) NiO/La_2O_3 catalyst precursors at different reaction temperatures. (GHSV = 12,000 h^{-1}).

H_2 produced from the CDM reaction. Therefore, the catalytic activity of $LaNiO_3$ perovskite gradually increased at the initial stage of reaction to the maximum when the $LaNiO_3$ perovskite phase was completely reduced to metallic nickel and La_2O_3. Subsequently the catalytic activity slightly decreased due to the formation of carbon deposits on the metallic nickel. On the other hand, Fig. 6(b) shows that the NiO/La_2O_3 catalyst precursor exhibited the maximum catalytic activities at the beginning of reaction due to the NiO phase which had been completely reduced prior to the reaction.

At 600 °C and 650 °C, both catalysts show the maximum CH_4 conversion of about 42% and 60%, respectively. The catalytic activities remain almost constant over the period of 5 h. Upon increasing the reaction temperatures, the maximum CH_4 conversion over $LaNiO_3$ perovskite catalyst reaches 65% at 700 °C, 80% at 750 °C, and 92% at 800 °C. After reaching the maximum CH_4 conversion, the activity of $LaNiO_3$ perovskite catalyst slightly decreases with time. Similar to $LaNiO_3$ perovskite catalyst, the increase of CH_4 conversion with reaction temperature is also observed with the NiO/La_2O_3 catalyst due to the characteristic of endothermic reaction. However, NiO/La_2O_3 catalyst deactivated much faster than $LaNiO_3$ perovskite catalyst at high reaction temperatures. For instance, NiO/La_2O_3 catalyst completely deactivated within 2 h, whereas $LaNiO_3$ perovskite is still highly active over the period of reaction (5 h) at 800 °C. These results show the advantage of $LaNiO_3$ perovskite over NiO/La_2O_3 catalyst, whereby $LaNiO_3$ perovskite could be able to perform at higher reaction temperature to achieve higher CH_4 conversion.

Fig. 7 shows the SEM images of carbon deposits on the used $LaNiO_3$ perovskite and NiO/La_2O_3 catalysts performed under CDM reaction at different temperatures. At low temperatures (600–700 °C), the used $LaNiO_3$ perovskite is completely covered by carbon filaments with highly uniform diameter. Besides the carbon filaments, small amount of carbon deposits with globular-like structure are also observed on the used $LaNiO_3$ perovskite catalyst performed at higher temperature of 800 °C. Similarly, carbon filaments are also observed on the used NiO/La_2O_3 catalysts at 600 °C, but their diameters are large and not as uniform as those formed on the used $LaNiO_3$ perovskite catalyst. Moreover, a large amount of globular carbon start to be observed on the used NiO/La_2O_3 catalyst performed at the reaction temperature higher than 600 °C. These results reveal that the formation of carbon filaments allow both catalysts to maintain their activity for methane decomposition, in spite of the increasing concentration of carbon deposited on the catalysts [9,10]. According to the mechanism of the formation of carbon filaments during CDM reaction, the Ni^0 particle at the tip of CNT is always clean enough to react with methane, thus leading to the continual catalytic process without catalytic deactivation. However, only the Ni^0 particles with diameter of 10–50 nm are able to form carbon filaments at moderate temperature [26]. Therefore, the large agglomerated Ni^0 particles (over 100 nm), which are formed after the H_2 reduction of NiO/La_2O_3 catalyst, are difficult to form carbon filaments, hence causing the rapid deactivation of NiO/La_2O_3 catalyst. On the other hand, the small Ni^0 particles (20–30 nm), which are formed after the H_2 reduction of $LaNiO_3$ perovskite, are able to form carbon filaments during the reaction, thus their activity can be maintained for a long reaction time.

3.2.1. *Influence of reaction temperature*

Besides the Ni^0 particle size, reaction temperature also substantially affects the catalytic performance. Fig. 6 shows that the deactivation rate is substantially increased with the increase of reaction temperature. The effect of reaction temperature on the catalytic performance can be explained by the difference between the decomposition rate of methane at the front surface of Ni^0 particles and the diffusion rate of dissolved carbon atoms through Ni^0 particles (Fig. 8). At low temperature, the decomposition rate of methane is rather slow and becomes the rate determining step for CDM reaction, hence resulting in the lower catalytic activity of both catalysts for H_2 production. As the reaction temperature is increased towards the optimum reaction temperature, the decomposition rate of methane and the diffusion rate of carbon atoms are increased till these two rates become balanced, leading to the continual growth process of carbon filaments without the formation of excess carbon. Therefore, the catalytic activity at the optimum reaction temperature can be maintained for a long period of reaction. Upon further increase of the reaction temperature, the decomposition rate of methane becomes much higher than the diffusion rate of carbon atom through Ni^0 particles. Consequently, the Ni^0 particles are rapidly covered by the excess carbon, forming carbon with globular-like structure (instead of filamentous structure) which causes the rapid deactivation of catalysts. Moreover, it is worth to note here that the difference between the methane decomposition rate and the carbon atom diffusion rate at high reaction temperature over the larger Ni^0 particle is much higher than those observed over the smaller Ni^0 particles. This is due to the fact that the larger Ni^0 particles not only have more active surface to decompose methane to H_2 and carbon atoms, but also have the longer distance for carbon atoms to diffuse through. Consequently, the larger Ni^0 particle is readily covered by the excess carbon and form globular-like structure at high reaction temperature. Therefore, it is not surprising that the large agglomerated Ni^0 particles (>100 nm) after the reduction of NiO/La_2O_3 catalyst are completely deactivated within 2 h at 800 °C.

3.2.2. *Influence of H_2 presence in the feed stream*

Fig. 9 shows the effect of the presence of H_2 in the feed stream on the catalytic performance of $LaNiO_3$ perovskite catalyst performed

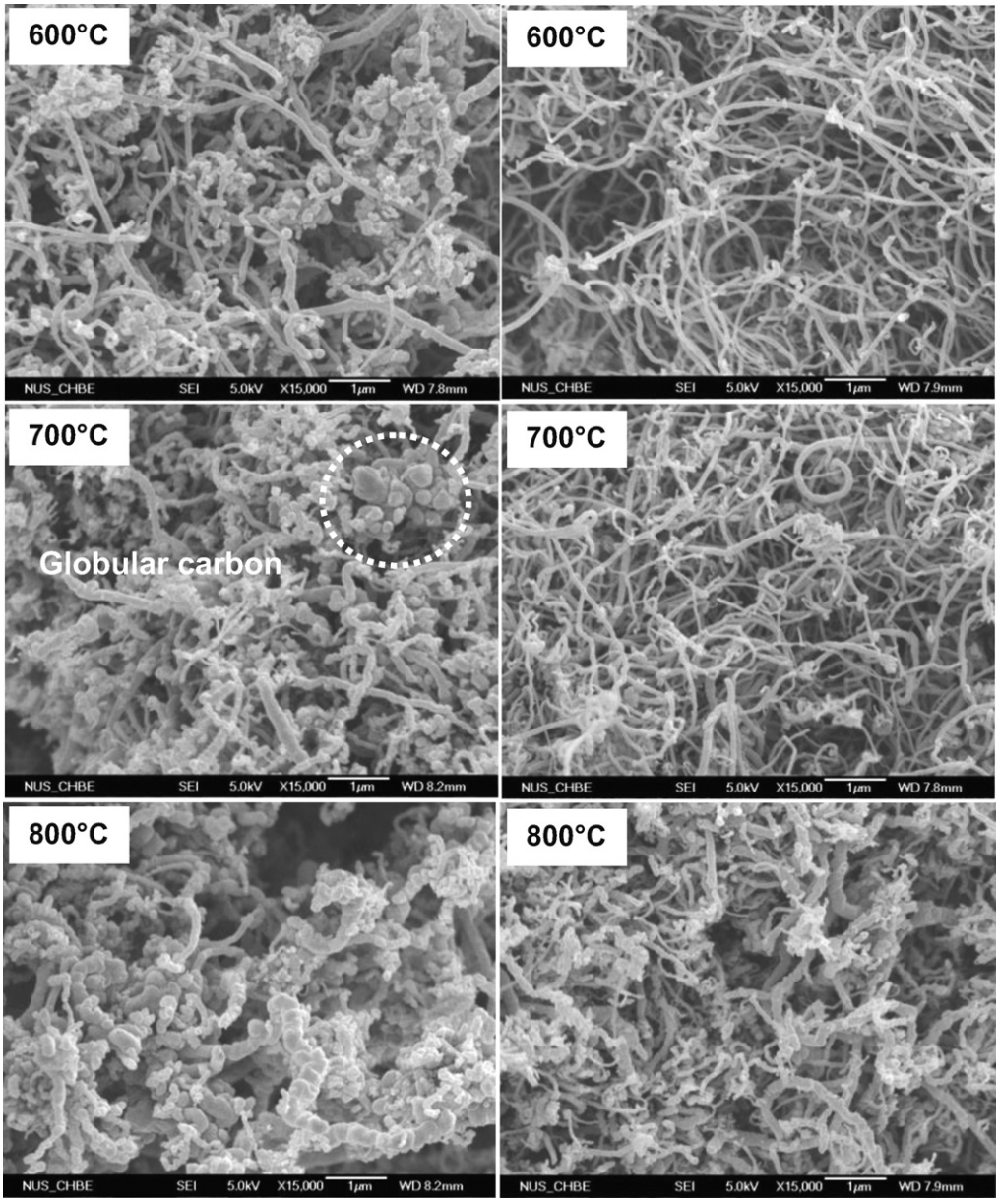

Fig. 7. SEM images of carbon deposits produced from CDM reaction over NiO/La_2O_3 (left) and $LaNiO_3$ perovskite catalyst precursors (right) at 600 °C, 700 °C, and 800 °C.

at three reaction temperatures, i.e. 600, 700 and 800 °C. It can be observed that the presence of H_2 in the feed stream significantly reduces the catalytic deactivation rate at high reaction temperature. This is because H_2 could clean the active surface of Ni^0 particles by H_2 gasification of the excess carbon ($C + 2H_2 \rightarrow CH_4$). This excess carbon is mostly formed on the surface of Ni^0 particles at high reaction temperature which causes the methane decomposition rate to be much faster than carbon atom diffusion rate.

3.3. Characterization of carbon deposits

3.3.1. X-ray diffraction analysis

The carbon deposits on the used catalysts were investigated by XRD analysis. Figs. 1(e) and 2(e) show that the highly ordered graphitic-structure carbon deposits are produced from the CDM reaction over the $LaNiO_3$ perovskite and NiO/La_2O_3 catalyst precursors, respectively. This highly ordered graphitic structure is evidenced by the strong diffraction peak at $2\theta = 26.1°$.

3.3.2. Microscopic analysis

The structure of carbon deposits on the used catalysts was further investigated by TEM. Fig. 10 shows that the central region of carbon deposits is hollow, displaying the structure of carbon nanotube (CNT). The presence of carbon deposits with rod-like structure (carbon nanofiber) and globular-like structure (encapsulating carbon) can also be observed, especially on the NiO/La_2O_3 catalyst performed at high reaction temperature. TEM images show that CNTs obtained from CDM reaction over $LaNiO_3$ perovskite catalyst have highly uniform diameter of 25.4 ± 5.84 nm. On the contrary, CNTs with very broad size (40.1 ± 24.12 nm) are obtained from CDM reaction over NiO/La_2O_3 catalyst.

The HR-TEM images (Fig. 11) show that the carbon deposits obtained from $LaNiO_3$ perovskite catalyst are produced in the form of multi-walled nanotubes (MWNTs). The graphitic layers are stacked parallel to the fiber axis and the interlayer distance between two adjacent graphitic layers is about 0.343 nm, which is higher than those observed in the perfect graphite (0.335 nm) [27]. The higher interlayer distance may be attributed to the

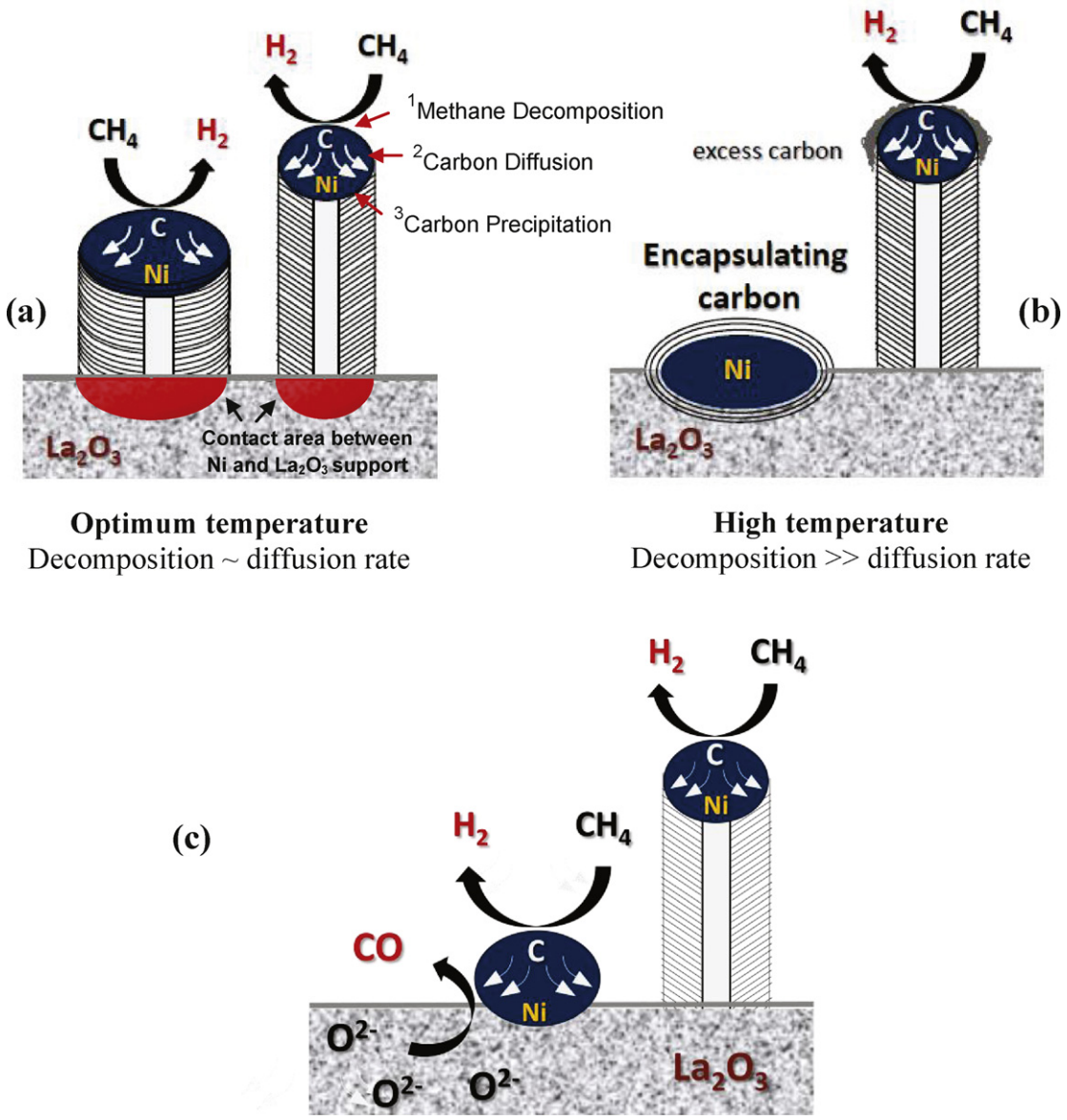

Fig. 8. Schematic representation of the formation of (a) carbon filaments, (b) encapsulating carbons and (c) the formation of CO via reaction between carbon atoms and lattice oxygen (O^{2-}) from the support at the beginning of reaction [Red areas in (a) represent contact areas between Ni^0 particles and La_2O_3 support before Ni^0 particles detach from La_2O_3 support]. (For interpretation of the references to color in this figure legend, the reader is referred to the web version of the article.)

curved-shape of CNTs, which induces strain inside the stacking of the graphitic layers. Fig. 11 also shows the crystallographic orientation of crystal faces on the Ni^0 particle. The crystal faces were assigned according to the studies by Yang et al. [9], who reported that for metal with fcc structure (such as Ni, FeCo and FeNi alloys), the metal–carbon interface consists of (1 1 1) crystal face. On the other hand, the metal–gas interface consists of (1 1 0) and (1 0 0) faces, which are highly reactive faces for CH_4 decomposition. That order is reversed for their activities for CO decomposition [28] since the (1 1 0) crystal face of conical particles coincides with the carbon tube axis, whereas the metal-gas interface consists of (1 1 1) crystal face and this face is reactive for CO decomposition. According to the studies by Yang et al. [9], it can be concluded that the decomposition of methane occurs on the front surfaces of Ni^0 particle having (1 0 0) and (1 1 0) faces, followed by the dissolution of carbon atoms into Ni^0 particles and diffusion through the Ni^0 particles. The dissolved carbon atoms then precipitate at the rear (1 1 1) face of the Ni^0 particles, consequently detach the Ni^0 particles from the La_2O_3 support and form a carbon nanotube with an exposed Ni^0 particle at its tip (Fig. 11(a)); this mechanism observed in our study follows the tip-growth mechanism.

There are two main different mechanisms (i.e. tip-growth and base-growth) which have been proposed for the growth of CNTs during CH_4 decomposition. Metal–support interaction is one of the most important factors which control the growth mechanism of carbon nanotube. In the base-growth mechanism, metal particles interact strongly with the support and remain pinned on the support during the growth of CNTs. It has been reported that iron-supported catalysts (such as Fe-supported on MgO, Al_2O_3, and SiO_2 [29]) mostly form CNTs via the base-growth mechanism, probably due to the strong metal–support interaction caused by the high thermal diffusion of Fe atoms into the support surface [30]. On contrary, in the tip-growth mechanism the growth of carbon nanotube, which involves the catalyst particle detached from the support and then located at the end of carbon nanotube, takes place when the metal–support interaction is weak. The presence of Ni^0 particle with conical shape at the tip of CNTs (Fig. 11(a)) obtained from both $LaNiO_3$ perovskite and NiO/La_2O_3 catalyst precursors confirm that

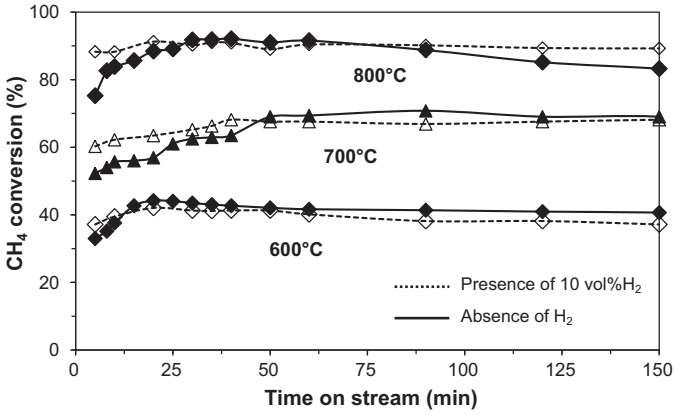

Fig. 9. Time on stream (TOS) vs. % CH_4 conversion over $LaNiO_3$ perovskite catalyst precursor in the presence of 10 vol% H_2 in the feed stream. (GHSV = 12,000 h^{-1}).

the growth of CNTs during CH_4 decomposition over both $LaNiO_3$ perovskite and NiO/La_2O_3 catalyst precursors takes place via the tip-growth mechanism.

However, the synthesis protocol of $LaNiO_3$ perovskite and NiO/La_2O_3 catalyst precursors has the major impact on morphology of Ni^0 particles deposited on La_2O_3 support after the reductive treatment. From TEM images (Fig. 5) of the reduced catalysts, it is possible to state that the larger Ni particles obtained from the reduction of NiO/La_2O_3 has a stronger physical interaction with La_2O_3 support, probably due to the larger contact area between the larger Ni^0 particles and La_2O_3 support (Fig. 8(a)). Although the stronger physical interaction between large Ni^0 particles with La_2O_3 support obtained from the reduction of NiO/La_2O_3 is not strong enough to attach Ni^0 particles to the support and form CNTs via the base-growth mechanism, it significantly causes the difficulty of Ni^0 particles to be detached from the support, making them susceptible to be covered by graphitic layer and formed encapsulating carbon especially at high reaction temperature. The HR-TEM images (Fig. 12) of the used NiO/La_2O_3 catalyst performed at 800 °C show that the Ni^0 particles are completely encapsulated by the highly ordered graphitic layers. Therefore, it is worth to note

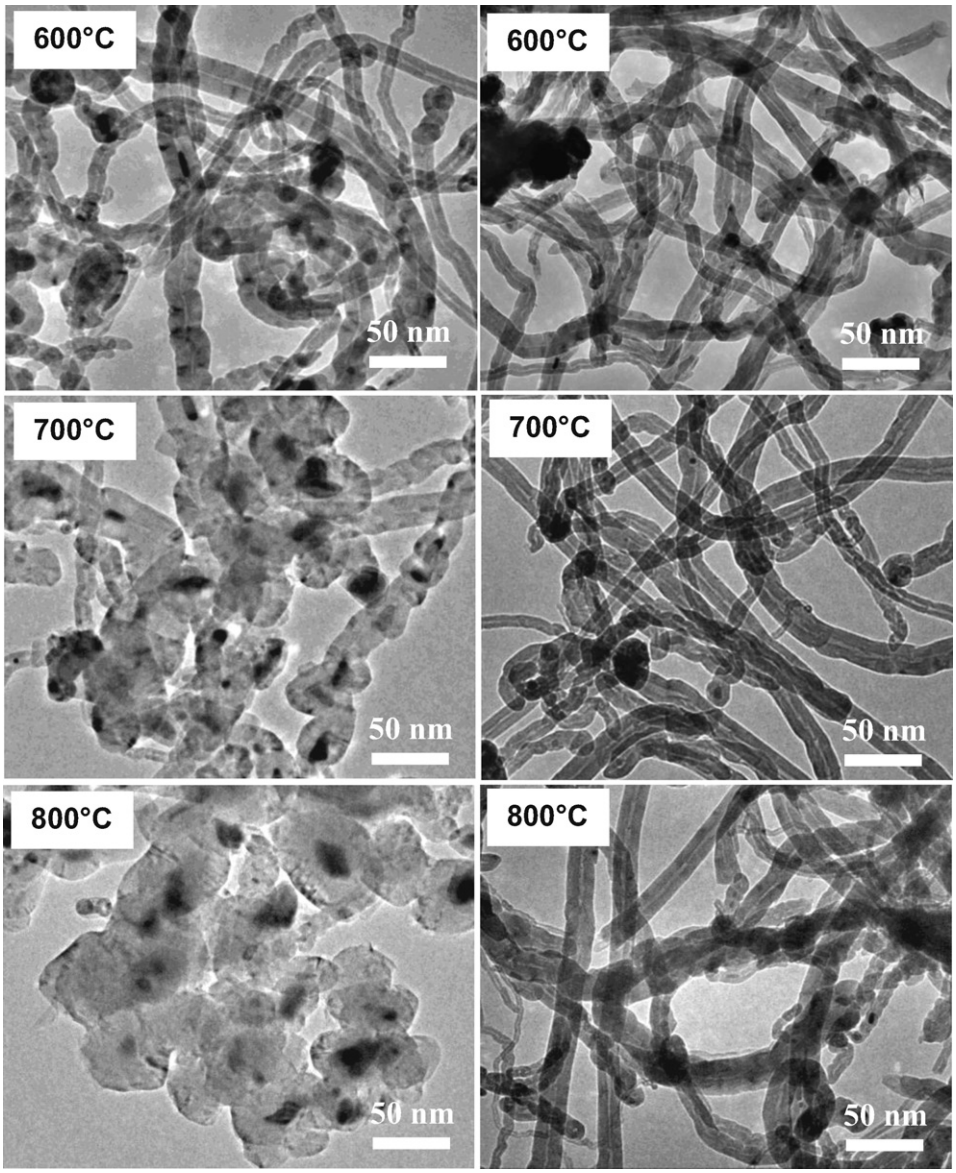

Fig. 10. TEM images of carbon deposits produced from CDM reaction over NiO/La_2O_3 (left) and $LaNiO_3$ perovskite catalyst precursors (right) at 600 °C, 700 °C, and 800 °C.

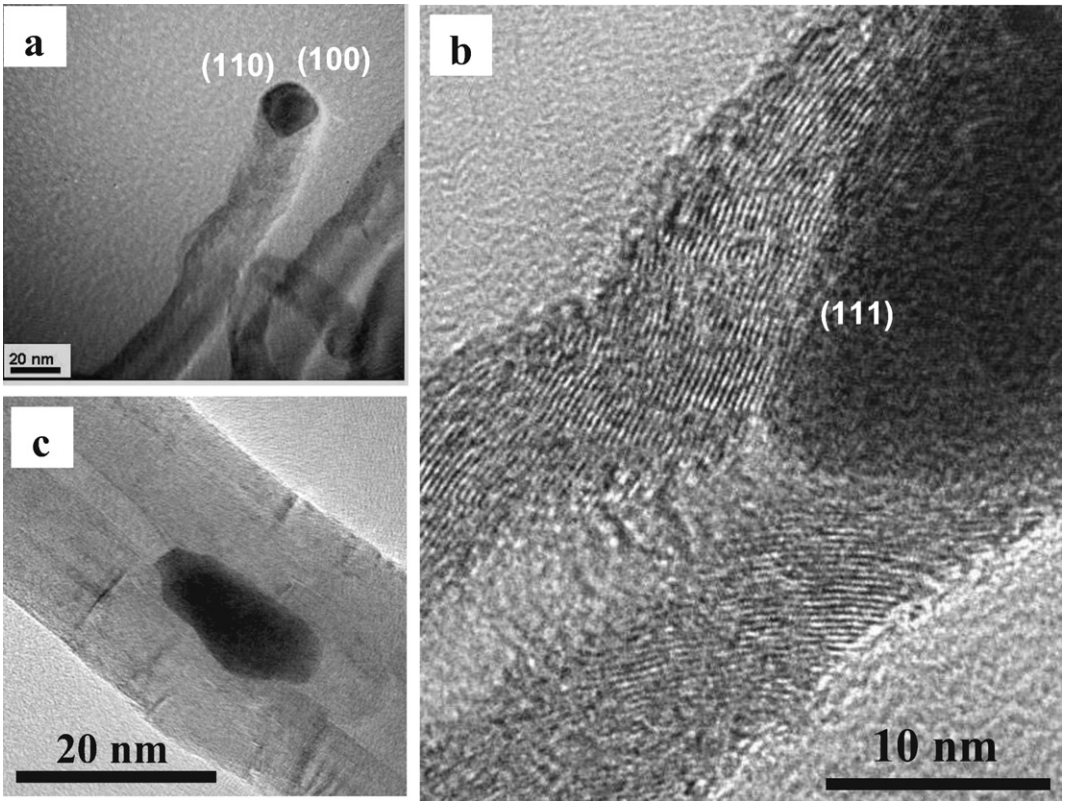

Fig. 11. HR-TEM images of CNTs produced from CDM reaction over $LaNiO_3$ perovskite and NiO/La_2O_3 catalyst precursors. (Crystallographic orientation of crystal plane was assigned relative to the studies of Yang et al. [9]: metal–gas interface at (1 1 0) and (1 0 0) planes, metal–carbon interface at (1 1 1) plane).

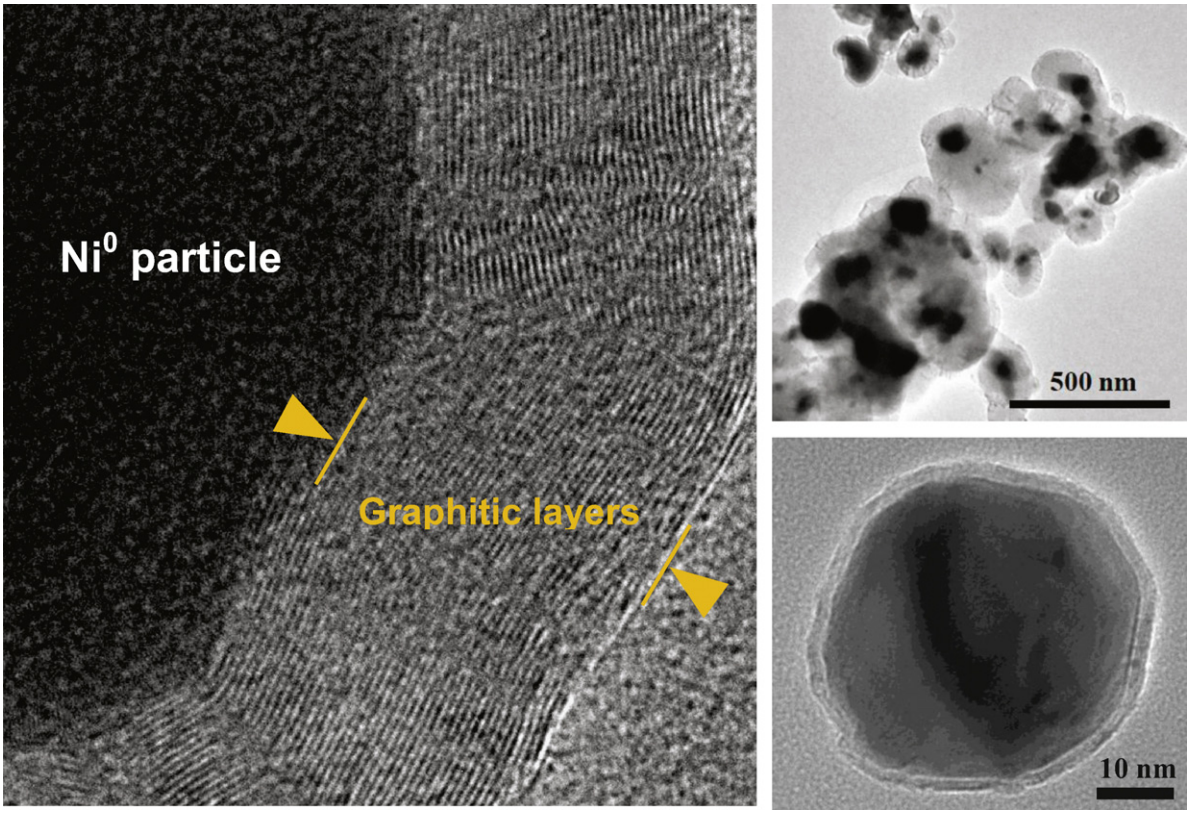

Fig. 12. HR-TEM images of encapsulating carbon produced from CDM reaction over NiO/La_2O_3 catalyst precursor at 800 °C.

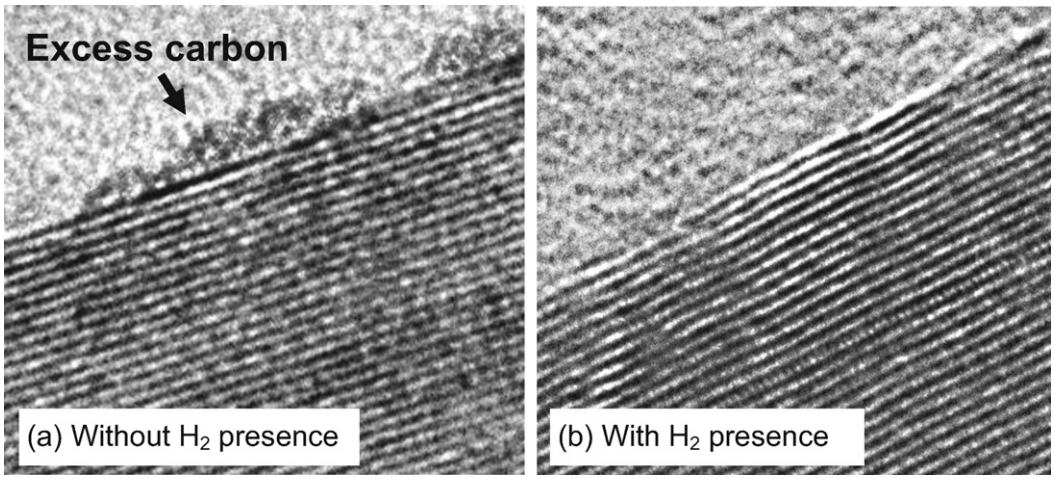

Fig. 13. HR-TEM images showing the presence of excess carbon on the surface of CNTs produced from CDM reaction over $LaNiO_3$ perovskite catalyst precursor at 800 °C.

that the formation of globular carbon (or encapsulating carbon) in which the active Ni^0 particles are embedded in the graphitic layers is the main reason for the rapid deactivation of NiO/La_2O_3 catalyst particularly at high reaction temperature, as mentioned earlier.

In addition to Ni^0 particle at the tip of CNT, some Ni^0 particle can sometimes be observed inside CNT since Ni^0 particle located at the tip of CNT can behave like a quasi-liquid particle under the reaction condition [31]. Therefore Ni^0 particle can be easily extruded and broken into smaller Ni particle which is then trapped inside CNT by the strong capillary force which usually occurs inside nanometer-sized cavities [32,33].

3.3.3. *Influence of H_2 presence in the feed stream on structure of CNTs*

Fig. 13 shows the TEM image of CNTs produced from CDM reaction over $LaNiO_3$ perovskite catalyst with and without the presence of H_2 in the feed stream at high reaction temperature. Besides the highly ordered graphitic layers, trace amount of amorphous carbon can also be observed on the surface of CNTs, especially over the $LaNiO_3$ perovskite catalyst. This is probably due to the difference between the decomposition rate of methane and the diffusion rate of carbon atoms at high reaction temperature which produces a lot of excess carbons that can migrate to the surface of CNTs. However, no amorphous carbon can be observed on the surface of CNTs when 10 vol% of H_2 was introduced into the feed steam.

Fig. 14 shows the O_2-TPO profiles of CNTs produced from CDM reaction at 800 °C over $LaNiO_3$ perovskite catalyst with and without the presence of H_2 in the feed stream. The small peak at 300–450 °C refers to the oxidation of amorphous carbon [34], confirming the presence of amorphous carbon on the surface of CNTs produced from CDM reaction over $LaNiO_3$ perovskite catalyst without the presence of H_2. The TPO peak at 467.9 °C observed on the CNTs produced from CDM reaction over $LaNiO_3$ perovskite catalyst without H_2 presence reveals the formation of CNTs with less ordered graphitic structure. However, the CNTs produced from CDM reaction over $LaNiO_3$ perovskite catalyst in the presence of H_2 have higher oxidation temperature (687.8 °C) than those CNTs produced without H_2 presence in the feed stream (662.9 °C). These results suggest that the presence of H_2 in the feed stream not only reduces the catalytic deactivation rate of $LaNiO_3$ perovskite catalyst at high reaction temperature by the removal of excess carbon atoms on the surface of Ni^0 particles via the H_2 gasification, but also helps to improve the ordered graphitic structure of CNTs [35].

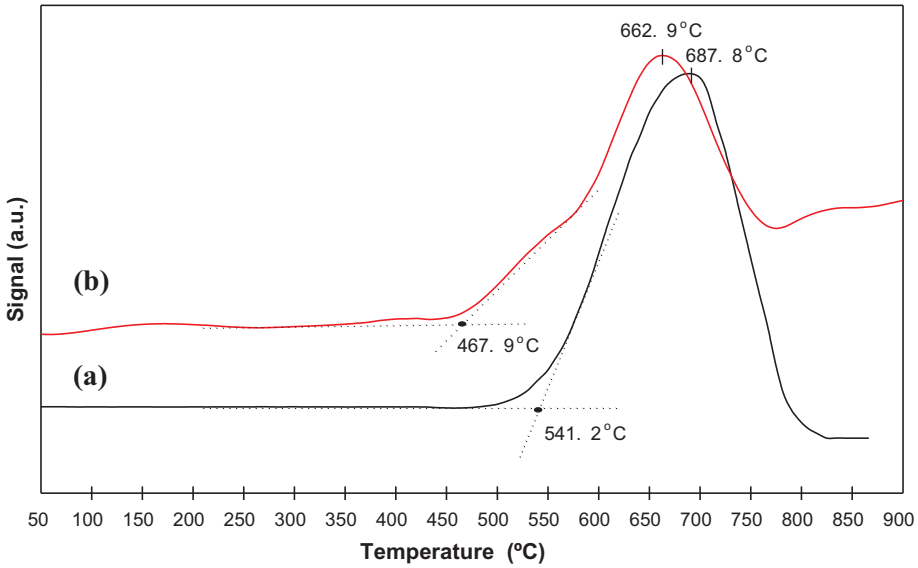

Fig. 14. O_2-TPO profiles of CNTs produced from CDM reaction over $LaNiO_3$ perovskite catalyst precursor at 800 °C in (a) the presence of 10 vol% H_2 and (b) the absence of H_2.

4. Conclusion

$LaNiO_3$ perovskite has been successfully used as a crystalline catalyst precursor for catalytic decomposition of methane with high activity and stability at high reaction temperature, due to the formation of uniform Ni^0 particles (24.00 ± 3.35 nm) which is able to form carbon filaments during the CDM reaction. On the other hand, the large agglomerated Ni^0 particles (40.78 ± 12.53 nm) from NiO/La_2O_3 are difficult to form carbon filaments, causing the rapid deactivation of catalyst. Moreover, the presence of H_2 in the feed stream not only reduces the deactivation rate of $LaNiO_3$ perovskite catalyst at high reaction temperature, but also eliminates amorphous carbon on the surface of CNTs and improves the ordered graphitic structure of CNTs.

Acknowledgements

The authors gratefully acknowledge the financial support from the National University of Singapore and A*STAR agency (SERC Grant 0921380022 and RO 279-000-292-305).

References

[1] G. Jones, J.G. Jakobsen, S.S. Shim, J. Kleisa, M.P. Andersson, J. Rossmeisl, F. Pedersen, T. Bligaard, S. Helveg, B. Hinnemann, J.R. Rostrup-Nielsen, I. Chorkendorff, J. Sehested, J.K. Norskova, J. Catal. 259 (2008) 147–160.
[2] G.S. Gallego, F. Mondragon, J. Barrault, J.M. Tatibouet, C.B. Dupeyrat, Appl. Catal. A: Gen. 311 (2006) 164–171.
[3] Y. Chen, W. Zhou, Z. Shao, N. Xu, Catal. Commun. 9 (2008) 1418–1425.
[4] S. Iijima, Nature 354 (1991) 56–58.
[5] N.M. Rodriguez, M.S. Kim, R.T.K. Baker, J. Phys. Chem. 98 (1994) 13108–13111.
[6] C. Park, E.S. Engel, A. Crowe, T.R. Gilbert, N.M. Rodriguez, Langmuir 16 (2000) 8050–8056.
[7] A. Chambers, C. Park, R.T.K. Baker, N.M. Rodriguez, J. Phys. Chem. B 102 (22) (1998) 4253–4256.
[8] H. Dai, J.H. Hafner, A.G. Rinzler, D.T. Colbert, R.E. Smalley, Nature 384 (1996) 147–150.
[9] R.T. Yang, J.P. Chen, J. Catal. 115 (1989) 52–64.
[10] L.S. Lobo, M.D. Franco, Catal. Today 7 (1990) 247–256.
[11] S. Takenaka, Y. Shigeta, E. Tanabe, K. Otsuka, J. Phys. Chem. B 108 (2004) 7656–7664.
[12] N.Z. Muradov, Int. J. Hydrogen Energy 18 (1993) 211–215.
[13] H.Y. Wang, E. Ruckenstein, Carbon 40 (2002) 1911–1917.
[14] T.V. Choudhary, C. Sivadinarayana, C.C. Chusuei, A. Klinghoffer, D.W. Goodman, J. Catal. 199 (2001) 9–18.
[15] S.H.S. Zein, A.R. Mohamed, Energy Fuels 18 (2004) 1336–1345.
[16] I. Suelves, M.J. Lazaro, R. Moliner, B.M. Corbella, J.M. Palacios, Int. J. Hydrogen Energy 30 (2005) 1555–1567.
[17] Q. Jiang, L.J. Song, Y. Zhao, X.Y. Lu, X.T. Zhu, L. Qian, X.M. Ren, Y.D. Cai, Mater. Lett. 61 (2007) 2749–2752.
[18] M.E. Rivas, C.E. Hori, J.L.G. Fierro, M.R. Goldwasserc, A. Griboval-Constant, J. Power Sources 184 (2008) 265–275.
[19] M.R. Goldwasser, M.E. Rivas, E. Pietri, M.J. Pérez-Zurita, M.L. Cubeiro, A. Grivobal-Constant, G. Leclercq, J. Mol. Catal. A: Chem. 228 (2005) 325–331.
[20] G. Valderrama, M.R. Goldwasser, C. Urbina de Navarro, J.M. Tatibouët, J. Barrault, C. Batiot-Dupeyrat, F. Martínez, Catal. Today 107–108 (2005) 785–791.
[21] E. Ruckenstein, Y.H. Hu, J. Catal. 161 (1996) 55–61.
[22] M. Kuras, Y. Zimmermann, C. Petit, Catal. Today 138 (2008) 55–61.
[23] W. Shen, F.E. Huggins, N. Shah, G. Jacobs, Y. Wang, X. Shi, G.P. Huffman, Appl. Catal. A: Gen. 351 (2008) 102–110.
[24] J. Ashok, S.N. Kumar, A. Venugopal, V.D. Kumari, M. Subrahmanyam, J. Power Sources 164 (2007) 809–814.
[25] L.B. Avdeeva, D.I. Kochubey, Sh.K. Shaikhutdinov, Appl. Catal. A: Gen. 177 (1999) 43–51.
[26] P.E. Nolan, D.C. Lynch, A.H. Cutler, J. Phys. Chem. B 102 (1998) 4165–4175.
[27] N.M. Rodriguez, A. Chambers, R.T.K. Baker, Langmuir 11 (1995) 3862–3866.
[28] M. Audier, M. Coulon, A. Oberlin, Carbon 18 (1980) 73–76.
[29] S. Fan, M.G. Chapline, N.R. Franklin, T.W. Tombler, A.M. Cassell, H. Dai, Science 283 (1999) 512–514.
[30] H. Ago, K. Nakamura, N. Uehara, M. Tsuji, J. Phys. Chem. B 108 (2004) 18908–18915.
[31] G. Gulino, R. Vieira, J. Amadou, P. Nguyen, M.J. Ledoux, S. Galvagno, G. Centi, C. Pham-Huu, Appl. Catal. A: Gen. 279 (2005) 89–97.
[32] M.R. Pederson, J.Q. Broughton, Phys. Rev. Lett. 69 (1992) 2689–2692.
[33] P.M. Ajayan, S. Ijima, Nature 361 (1993) 333–334.
[34] C. Li, K. Yao, J. Liang, Appl. Catal. A: Gen. 261 (2004) 221–224.
[35] P.E. Nolan, D.C. Lynch, A.H. Cutler, Carbon 32 (1994) 477–483.